

RESEARCH

Open Access



Melanin-intercalated layered double hydroxide LDH/MNP as a stable photothermal agent

Xue Li^{1,2}, Yixuan Wang³, Xinkai Geng³, Jinghua Sun³, Yulong Liu⁴, Anjie Dong¹ and Ruiping Zhang^{5*}

Abstract

Melanin nanoparticles (MNPs) are a type of electronegative compound that can be used as photothermal agent for cancer treatment. Nevertheless, the agglomeration of MNP, which is one of the limitations in practice, contributes to the instability of MNP. Pristine layered double hydroxide (LDH), as a kind of positive inorganic material when there exist no other cargo between its layers, can accommodate electronegative molecules between its layers to endow them with stable properties. Hence, in this study, electronegative MNP was intercalated into LDH lamellas via ion-exchange method to obtain the stable original photothermal agent LDH/MNP, solving the tough problem of MNP's agglomeration. The surface morphology, X-ray diffraction and fourier transform infrared spectra affirmed the successful intercalation of MNP between LDH lamellas. The Z-average particle sizes of LDH/MNP on day 0, 7 and 14 were measured as 221.8 nm, 227.6 nm and 230.5 nm without obvious fluctuation, while the particle sizes of MNP went through dramatic enlargement from 105.8 nm (day 0) to 856.1 nm (day 7), indicating the better stability of LDH/MNP than MNP. The typical polymer dispersity index (PDI) values on day 0, 7 and 14 verified the better stability of LDH/MNP, too. Photothermal properties of LDH/MNP were assessed and the results ensured the representative photothermal properties of LDH/MNP. The fine cytocompatibility of LDH/MNP was verified via cytotoxicity test. Results confirmed that the agglomeration of MNP disappeared after its intercalation into LDH and LDH/MNP possessed fine stability as well as typical photothermal property. The intercalation of MNP into LDH gave the photothermal agent MNP a promising way for its better stability and long-term availability in photothermal treatment.

Keywords Melanin, Layered double hydroxides, Stability, Photothermal therapy

*Correspondence:

Ruiping Zhang
zrp_7142@sxmu.edu.cn

¹Department of Polymer Science and Engineering, Key Laboratory of Systems Bioengineering (Ministry of Education), School of Chemical Engineering and Technology, Tianjin University, Tianjin 300072, China

²Department of Chemistry, School of Basic Medicine, Shanxi Medical University, Shanxi 030001, China

³The First Clinical Medical College of Shanxi Medical University, Shanxi 030001, China

⁴Shanxi Bethune Hospital, Third Hospital of Shanxi Medical University, Shanxi Academy of Medical Sciences, Tongji Shanxi Hospital, Taiyuan 030032, China

⁵The Radiology Department of Shanxi Provincial People's Hospital, Fifth Hospital of Shanxi Medical University, Shanxi 030001, China



© The Author(s) 2024. **Open Access** This article is licensed under a Creative Commons Attribution-NonCommercial-NoDerivatives 4.0 International License, which permits any non-commercial use, sharing, distribution and reproduction in any medium or format, as long as you give appropriate credit to the original author(s) and the source, provide a link to the Creative Commons licence, and indicate if you modified the licensed material. You do not have permission under this licence to share adapted material derived from this article or parts of it. The images or other third party material in this article are included in the article's Creative Commons licence, unless indicated otherwise in a credit line to the material. If material is not included in the article's Creative Commons licence and your intended use is not permitted by statutory regulation or exceeds the permitted use, you will need to obtain permission directly from the copyright holder. To view a copy of this licence, visit <http://creativecommons.org/licenses/by-nc-nd/4.0/>.

Introduction

Cancer therapy still remains a medical challenge worthy of in-depth research at present. The current treatments for cancer consist of surgical resection, chemotherapy [1, 2], immunotherapy [3–5] and photothermal therapy [6–8]. Especially, photothermal agents were routinely utilized in photothermal therapy (PTT) with excellent photothermal conversion properties to convert light energy into heat energy under the irradiation of external light source efficiently in order to achieve cancer cell ablation. For example, the inorganic metal nano-material Au–Ag alloy exhibited a significant integrated high-quality photothermal feature with high photothermal conversion efficiency (80.4%) in the near-infrared region [9], the carbon-based nanoparticle such as graphene [10], graphite [11] and carbon nanotubes (CNTs) [12] were also widely used because of their low cost and abundance. Furthermore, the organic compound indocyanine green (ICG) [13] with a large π -conjugated system for absorbing NIR light could efficiently converting the light into thermal energy, too. With the advantages of low-grade invasion, easy to implement and selective local treatments, PTT tend to be an effective method for cancer treatments [14–16].

Melanin nanoparticles (MNP, $C_{18}H_{10}N_2O_4$) are a kind of endogenous pigment that can be widely found in organisms and possess fine biocompatibility. Besides, MNP can efficiently convert light energy into heat energy under near-infrared light source to achieve photothermal therapy [17–20]. Therefore, MNP, as a common photothermal agent, is widely used in the study of tumor photothermal treatments. However, the agglomeration of MNP is of common occurrence due to the hydrophobicity caused by its special molecular structure [21]. The instability of MNP gives the limitation to the application of MNP in photothermal therapy which may reduce the photothermal treatment efficiency and decrease the retention time in vivo, etc. Herein, suitable modification for MNP aiming to decrease its agglomeration and improve the stability of MNP is urgently needed.

Moreover, inorganic compounds are also the focus on research [22, 23]. Layered double hydroxides (LDHs) are inorganic materials composed of stacked positively charged layers with intercalated anions, ensuring

electrical neutrality. The structural formula of LDH can be expressed as $[M^{II}_n M^{III}(\text{OH})_{2+2n}]^+(\text{Am}^-)_{1/m} \times \text{H}_2\text{O}$ ($n=2-4$) [24]. LDH possesses a regular hexagonal structure with numerous hydrophilic -OH groups on its host layers. The interlayer of LDH can accommodate electronegative guests, making it applicable in various fields such as biological materials [25–27], wastewater purification [28–32], and electrochemistry [33–36]. In this research, via hydrothermal method, Mg–Al LDH was synthesized in which the center of the structure was Mg^{2+} , the six vertices were OH^- , and the unit layer was formed by the shared edge of the adjacent MgO_6 octahedron. Mg^{2+} located on the layer was replaced by Al^{3+} isomorphism in a certain range, which made the host layer with permanent positive charge. Then, the electronegative MNP was intercalated between the positive-charged lamellas of LDH by ion exchange method (Scheme 1). Herein, LDH was employed as the carrier of MNP, which was the solution for the agglomeration of MNP. It was the first time that LDH/MNP been investigated and there was no other photothermal agents ever been intercalated between LDH layers for the purpose of photothermal therapy. The intercalation of MNP was confirmed by morphology, X-ray diffraction and fourier transform infrared spectrum testing. The particle size distribution and PDI values of MNP and LDH/MNP at different times of day 0, day7 and day 14 were evaluated. The zeta potentials of LDH, MNP and LDH/MNP were tested, too. Typical photothermal properties of LDH/MNP were studied via certain photothermal experiments and the biocompatibility of LDH/MNP was assessed by cytotoxicity assay.

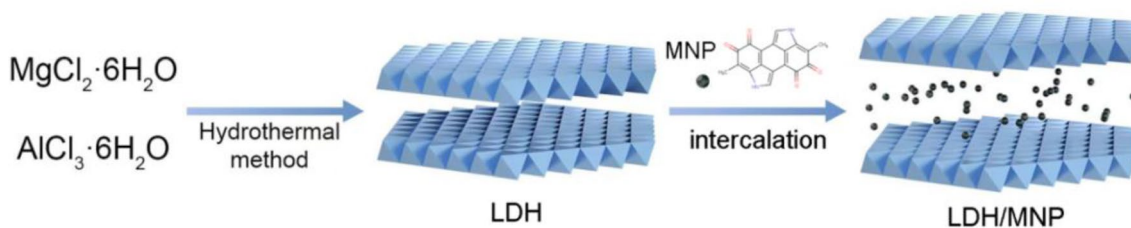
Experimental

Materials

$\text{MgCl}_2 \cdot 6\text{H}_2\text{O}$, $\text{AlCl}_3 \cdot 6\text{H}_2\text{O}$ and NaOH were purchased from Aladdin Corporation, China. Melanin was obtained from Sigma-Aldrich, St. Louis, MO, USA.

Preparation of Mg–Al LDH

The synthesis of Mg–Al LDH was conducted by hydrothermal method reported before [32]. Briefly, 10 mL $\text{MgCl}_2 \cdot 6\text{H}_2\text{O}$ (3.0 mmol) and 10 mL $\text{AlCl}_3 \cdot 6\text{H}_2\text{O}$ (1.0 mmol) solutions were mixed uniformly. Afterwards,



Scheme 1 The synthesis route of LDH/MNP

40 mL NaOH (0.15 mol/L) was added dropwise under nitrogen atmosphere. The mixture was kept stirring for 20 min. Next, the above mixture was centrifuged and washed using deionized water for three times. Finally, the precipitate was removed into the hydrothermal reactor for reaction at 100 °C for 16 h. The Mg-Al LDH suspension was obtained and lyophilized for 48 h.

Preparation of melanin nanoparticle (MNP)

MNP was prepared according to the previous reported method [37]. Generally, 0.1 mol/L NaOH was added into a brown bottle containing 20 mg of melanin and ultrasonic shock was conducted for 30 min until the mixture was completely dissolved. Then, the mixture was placed under the environment of 0 °C and 0.1 mol/L HCl was added dropwise until the mixture pH reached 7. Ultrafiltration centrifuge tube was used to centrifuge the mixture to about 1 mL. Subsequently, melanin nanoparticles were obtained by freeze-drying for 48 h.

Preparation of LDH/MNP

The intercalation of MNP between LDH layers was realized by ion exchange method. In short, 20 mg of melanin was uniformly dispersed in 20 mL of deionized water, and the above dispersions was added dropwise into 20 mL of 1 mg/mL LDH solution at 60 °C under nitrogen atmosphere. The mixture was kept stirring for 24 h. Afterwards, the product was freeze-dried for 48 h.

Characterization studies

Surface morphology analysis

The surface morphologies of LDH and LDH/MNP were observed by transmission electron microscopy JEM100C XII (Electronic Corporation, Japan). Briefly, the dispersions of LDH and LDH/MNP (1 mg/mL) were dropwise added to the copper mesh, after drying at 25 °C for 48 h, the copper mesh was removed under transmission electron microscopy to observe the surface morphology.

X-ray diffraction (XRD) analysis

The crystal characteristics of LDH and LDH/MNP were observed by DX-27mini X-ray diffract meter (Dandong Haoyuan Instrument, China) with Cu target (wavelength 0.154 nm). The powder sample of LDH and LDH/MNP was evenly spread on the sample plate and the scanning was set at pace of 4 °/min, the scanning range was 5 ° to 80 ° (2θ) and the ambient temperature was 25 °C.

Fourier transform infrared spectroscopy (FT-IR) analysis

The FT-IR test was performed with the TENSOR II infrared spectrometer (Bruker Corporation, German). Briefly, the KBr was mixed with the powder sample of LDH and LDH/MNP (mass ratio 100:1) and pressed after grinding respectively. The test range was set from 500 cm⁻¹ to

4000 cm⁻¹. The analysis was performed at room temperature of 25 °C.

Particle size and zeta potential measurement

The particle size and zeta potential of MNP and LDH/MNP were measured using Zetasizer Nano-ZS90 (Malvern Instrument, Inc., UK). The wavelength was 677 nm and the constant Angle was 90°. The measurements were repeated three times at room temperature and the average values were adopted. The concentration of MNP and LDH/MNP suspensions were 1 mg/mL. The zeta potentials of LDH, MNP and LDH/MNP were tested under the same experiment condition too.

Photothermal characterization of LDH/MNP in vitro

The photothermal conversion properties and photothermal stability of LDH/MNP was evaluated as follows. The LDH/MNP dispersions with different concentrations of 300/150/100/50/25/0 µg/mL and LDH dispersions of 100 µg/mL were put into containers and irradiated by laser (wavelength 808 nm, power density 1 W·cm⁻²) for 5 min, respectively. The real-time temperatures of the solutions were recorded every 15 s using an infrared thermal imager. After then, the LDH/MNP dispersions of 100 µg/mL were irradiated with different laser power densities (0.5/0.75/1.0/1.25 W·cm⁻²), and the real-time temperatures of the solution were recorded at an interval of 15 s using an infrared thermal imager, too. The LDH/MNP dispersions with a concentration of 100 µg/mL were irradiated with laser (wavelength 808 nm, power density 1 W·cm⁻²) for 5 min, and cooled naturally for 5 min then. The above 10 min was set as one cycle and the LDH/MNP dispersions were irradiated continuously for 6 cycles. The real-time temperature of the solution was recorded at an interval of 15 s to obtain the photothermal stability of LDH/MNP.

Cytotoxicity of LDH and LDH/MNP

The in vitro cytocompatibility of LDH and LDH/MNP was determined by Cell Counting Kit-8 (CCK-8) (GlpBio Corporation, USA). Normal cells H9C2 were inoculated into a 96-well plate and cultured in a cell incubator with 5% CO₂ at 37 °C for 24 h. Afterwards, 10 µL of LDH and LDH/MNP dispersions with different concentrations of 1000 µg/mL, 500 µg/mL, 250 µg/mL and 100 µg/mL were added respectively and incubated for 24 h, afterwards 10 µL CCK-8 solutions were added to the 96-well plate. After incubation for 4 h, cell absorption was detected at 450 nm by microplate reader.

Results and discussion

Surface morphology of LDH and LDH/MNP

The transmission electron microscopy micrographs of LDH and LDH/MNP were showed in Fig. 1. It could be

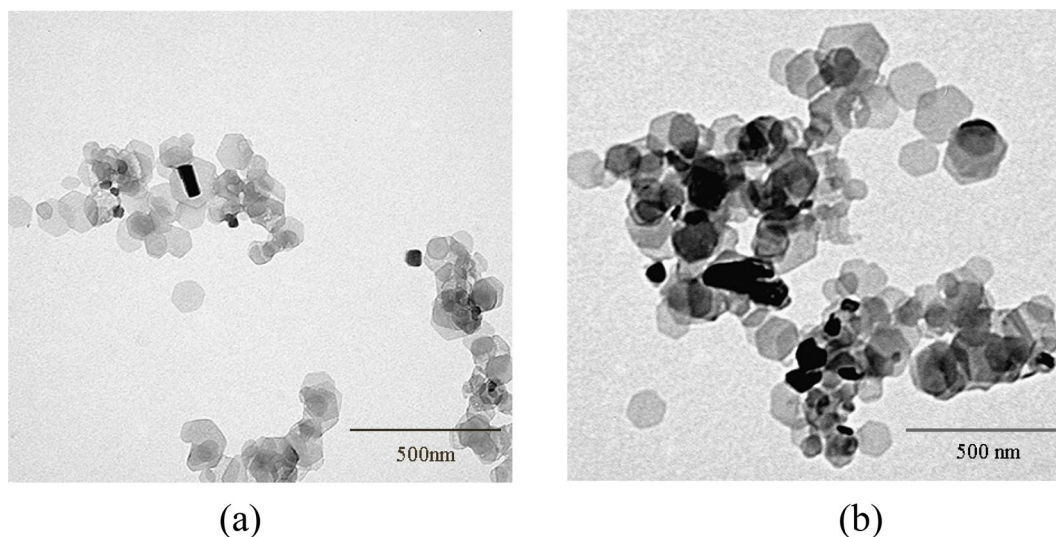


Fig. 1 TEM micrographs of LDH (a) and LDH/MNP (b)

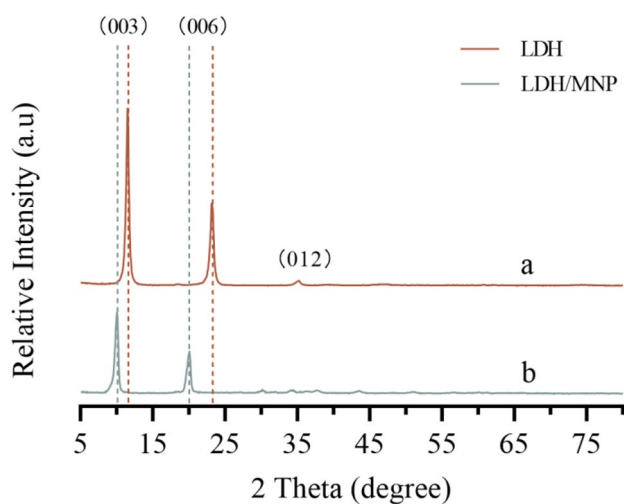


Fig. 2 XRD patterns of LDH and LDH/MNP. Scan angle from 5° to 80° (2 θ), leg speed 4°/min

observed via Fig. 1(a) that LDH presented regular hexagon structure with fine dispersion and the average particle size of LDH was around 100 nm. In Fig. 1(b), LDH/MNP nanoparticles also appeared a relatively fine particle distribution with the average particle size of 200 nm. In addition, it could be obviously observed that the color of most LDH/MNP was darker than that of LDH which was caused by the intercalation of the black-colored MNP. Besides, it could be seen from Fig. 1(b) that the edges of LDH/MNP nanoparticles became slightly smooth compared with LDH.

X-ray diffraction (XRD) analysis of LDH and LDH/MNP

The X-ray diffraction patterns of LDH (a) and LDH/MNP (b) in Fig. 2 were presented to clarify the crystallization and the intercalation of MNP. The diffraction peaks of

LDH at 11.48° (003), 23.18° (006) and 35.18° (012) were the typical characteristic peaks of LDH [38, 39]. After the intercalation of MNP between LDH layers, the typical peak of (003), (006) and (012) shifted left to the angle of 10.04°, 20.06° and 34.10°. The peak at low angle regions of (003) reflection related to the basal spacing between the layers and the interlayer spacing d_{003} of LDH and LDH/MNP could be calculated from the Bragg's Law ($2d\sin\theta = n\lambda$; $n = 1$, $\lambda = 0.154$ nm) as 0.7699 nm and 0.8799 nm respectively. The results ensured the increasing of the interlayer spacing after the intercalation of MNP into the pristine LDH and this was because the melanin possessed the bigger molecule size than the Cl^- and CO_3^{2-} in the pristine LDH. The increasing spacing of LDH/MNP showed the successful intercalation of MNP between LDH interlamination.

Besides, the relative intensity of characteristic diffraction peaks in Fig. 2a performed stronger than that in Fig. 2b. Specifically, the stronger XRD intensity of pristine LDH was due to its regular hexagonal structure without any impurities. However, when MNP intercalated, the space between the LDH layers became wider and MNP could be seen as the impurity for pristine LDH, leading to the weaker relative intensity of LDH/MNP. The relative intensities of LDH and LDH/MNP were consistent with the TEM micrographs in Fig. 1 and the weakened crystalline form of LDH/MNP corresponded to the roundish shape of LDH/MNP.

Fourier transform infrared spectroscopy (FT-IR) analysis of LDH, MNP and LDH/MNP

Fourier Transform Infrared (FT-IR) spectra of LDH, MNP and LDH/MNP were shown in Fig. 3 to further confirm the existence of MNP in LDH/MNP. With regard

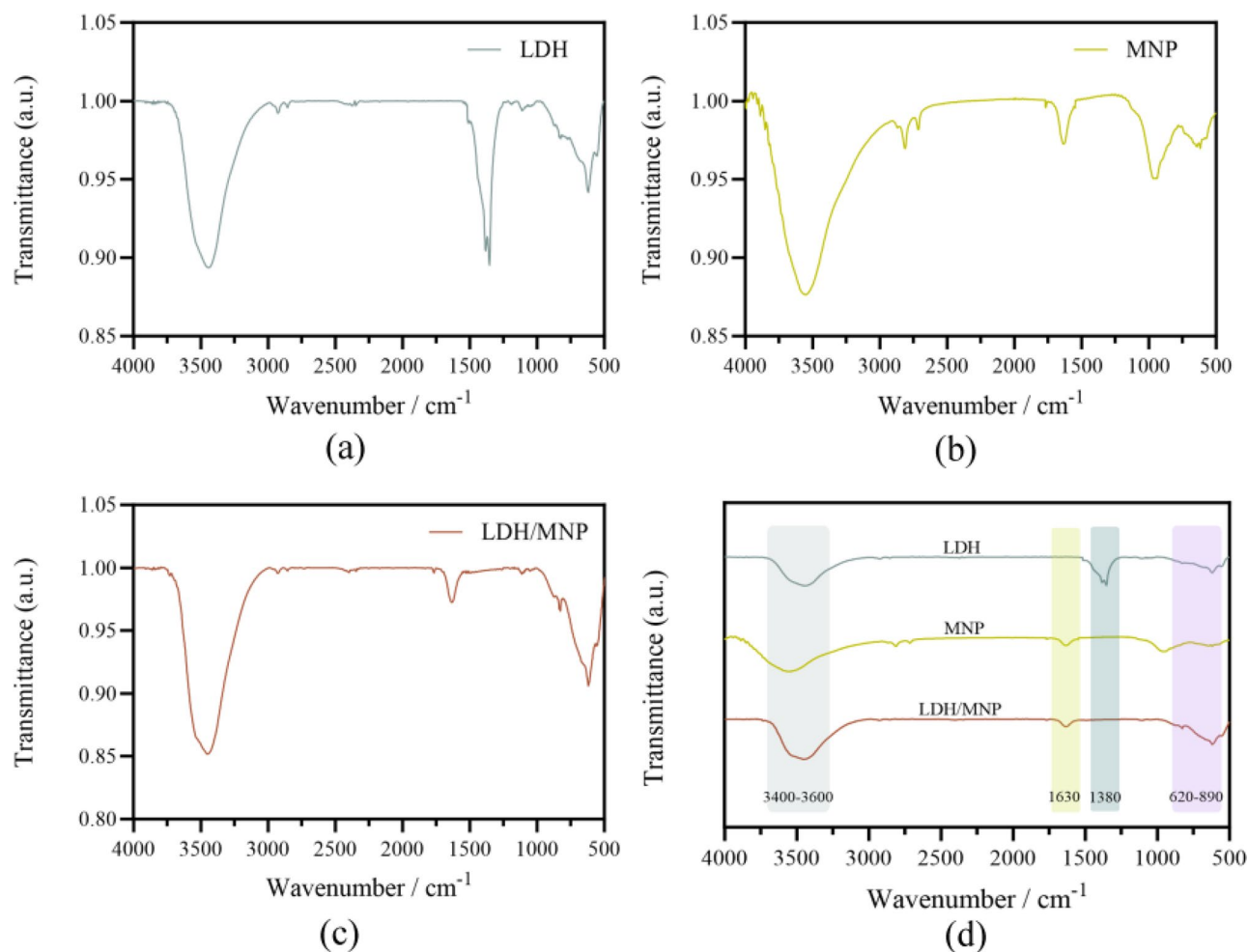


Fig. 3 FT-IR spectra of LDH (a), MNP (b), LDH/MNP (c) and the summarized FT-IR spectra of LDH, MNP and LDH/MNP (d). Region from 4000 cm⁻¹ to 500 cm⁻¹. The test of the powders was carried out by using KBr disks and test temperature was 25 °C

to LDH in Fig. 3(a), the strong broad absorption band at 3400 cm⁻¹ to 3600 cm⁻¹ belonged to the stretching vibration of the -OH groups on LDH laminates [40, 41]. The narrow and strong absorption peaks at 1380 cm⁻¹ could be ascribed to the asymmetric stretch vibration caused by CO₃²⁻ groups existed between LDH layers [42, 43]. The wide absorption band at 620 cm⁻¹ to 890 cm⁻¹ referred to the metal-oxygen-metal and oxygen-metal-oxygen stretching from LDH laminates [44, 45]. For the FT-IR spectra of MNP in Fig. 3(b), there was a broad absorption band at 3400 cm⁻¹ to 3600 cm⁻¹, generated by the stretching vibration of O-H and the stretching vibration of N-H from the indole structure of melanin [45]. The absorption peak observed at 1630 cm⁻¹ was derived from the characteristic absorption peak of aromatic groups C=O and C=C from MNP [45], which was a characteristic absorption peak of melanin. The band around 900 cm⁻¹ was attributed to the C-H bending vibration among the ring structure of the benzene in MNP. In the FT-IR spectra of LDH/MNP, the characteristic peak

belonged to MNP at 1630 cm⁻¹ was observed, indicating the existence of MNP. The characteristic absorption peaks of LDH at 3400 cm⁻¹ to 3600 cm⁻¹ and 620 cm⁻¹ to 890 cm⁻¹ were observed, too, indicating the existence of LDH. In addition, the wider and stronger absorption band in the FTIR spectra of LDH/MNP in the range of 3400–3600 cm⁻¹ may caused by the accumulation of both stretching vibration of O-H and stretching vibration of N-H within LDH and MNP. No absorption peak at 1380 cm⁻¹ was observed which illustrated that the CO₃²⁻ groups between the pristine LDH layers were replaced by MNP via ion exchange [47, 48]. Moreover, the band around 900 cm⁻¹ in Fig. 3(b) had almost disappeared in Fig. 3(c). This was because that the bending vibration of C-H was extremely susceptible to external influences and when the MNP intercalated between the LDH layers, the bending vibration of C-H was weakened by the interaction between MNP and the laminates of LDH. As a consequence, the disappearing of the band at 900 cm⁻¹ could laterally prove the intercalation of the MNP between

LDH layers. The FT-IR results confirmed the existence of MNP and LDH in the system of LDH/MNP. Combined with the XRD results in Fig. 2, the intercalation of MNP between LDH layers could be verified in LDH/MNP.

Particle size of MNP and LDH/MNP on day 0, 7 and 14

The stability of MNP and LDH/MNP was evaluated via the particle size distributions and PDI values. The particle sizes of MNP and LDH/MNP dispersed in PBS on day 0, 7 and 14 were showed respectively in Fig. 4(a) and Fig. 4(b). As shown in Fig. 4(a), the particle size distribution of MNP performed huge differentiation on day 0, 7 and 14 while the particle size distribution of LDH/MNP in Fig. 4(b) exhibited unapparent change, illustrating the fine stability of LDH/MNP. In Fig. 4(c), the average particle sizes of MNP were 105.8 nm, 856.1 nm and 2673 nm on day 0, 7 and 14 respectively. The abnormal particle enlargement of MNP was observed on day 7 and the larger particle size was not conducive to realize endocytosis. Therefore, according to the particle size on day 7, which was 856.1 nm, the MNP cannot be employed as a

suitable photothermal agent anymore. However, the average particle size of LDH/MNP was 221.8 nm, 227.6 nm and 230.5 nm on day 0, 7 and 14 respectively. The particle size of LDH/MNP was consistent with the TEM micrograph results of LDH/MNP in Fig. 1(b). The stable unchanged particle sizes on different days indicated that the LDH/MNP held fine stability and LDH/MNP was free of agglomeration. Polymer dispersity index (PDI) commonly indicated the molecular weight distribution and it was inversely proportional to molecular weight distribution. In Fig. 4(d), the PDI values of MNP on day 0, 7 and 14 were tested as 0.448, 0.576 and 1 respectively. The results in Fig. 4(d) revealed that the distribution of MNP had become uneven gradually as time passed. However, for LDH/MNP, the PDI values on day 0, 7 and 14 were 0.054, 0.107 and 0.173, performing no major changes basically. The stable PDI values manifested the fine particle distribution of LDH/MNP. The gradually increasing particle size and suboptimal distribution of MNP from day 0 to day 14 were caused by the hydrophobicity of MNP. Concretely, there were conjugated systems

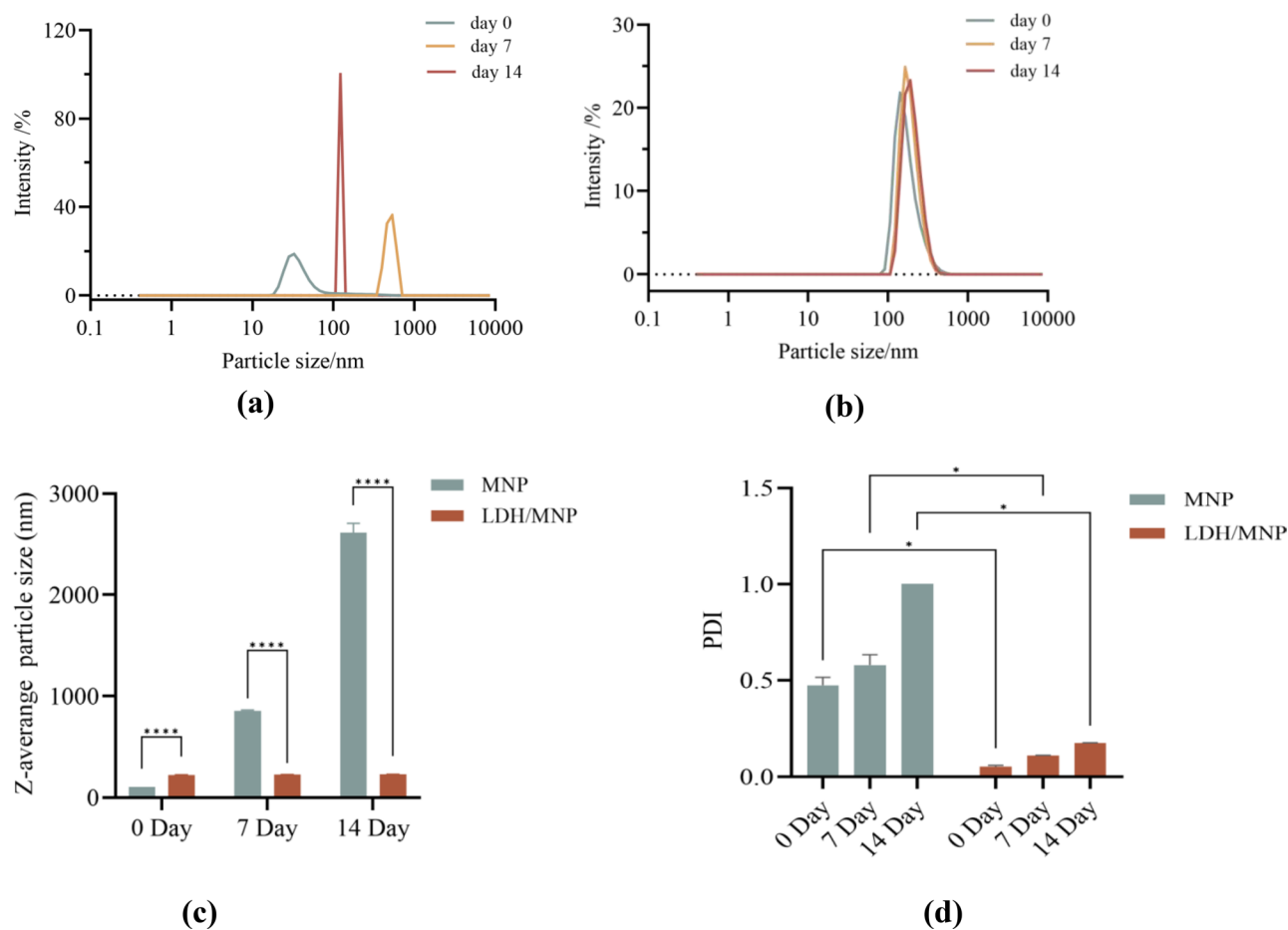


Fig. 4 Size distributions of MNP (a) and LDH/MNP (b) dispersed in PBS on day 0, 7 and 14 with the concentration of 1 mg/mL; (c) Z-average particle sizes of MNP and LDH/MNP dispersed in PBS on day 0, 7 and 14 with the concentration of 1 mg/mL; (d) Polymer dispersity index (PDI) values of MNP and LDH/MNP dispersed in PBS on day 0, 7 and 14 with the concentration of 1 mg/mL

in the major molecular structure of MNP which was non-polar (Scheme 1). This nonpolar structure rendered MNP the hydrophobicity property in aquatic environment. As a result, the separated hydrophobic groups tended to aggregate together, resulting in the poorer particle distribution of MNP over time. However, when the electronegative MNP intercalated between the interlamellar spaces of LDH by swapping out the original less electronegative Cl^- and CO_3^{2-} via ion exchange method, LDH/MNP became stable in aquatic environment because of the huge number of hydroxyl groups on the surface of LDH layers while at the same time the hydrophobic groups of MNP were wrapped in LDH. Hence, after the intercalation of MNP, LDH/MNP possessed better dispersion and stability than MNP and the particle size of LDH/MNP maintained ~ 200 nm within 14 days.

Zeta potential of LDH, MNP and LDH/MNP

As the testing results in Fig. 5, the average zeta potentials of LDH and MNP were $+35.3$ mv and -30.0 mv respectively, declaring that MNP could intercalate into the LDH layers by ion exchange way. Moreover, after the

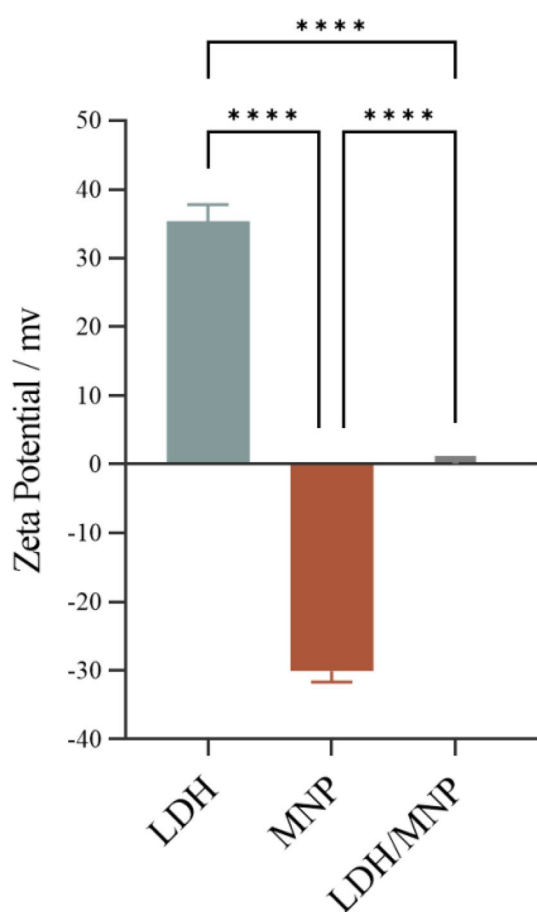


Fig. 5 Zeta potential of LDH, MNP and LDH/MNP with the concentration of 1 mg/mL

intercalation of MNP into LDH layers, the average zeta potential of synthesized LDH/MNP had decreased to 0.06 mv, indicating the electro neutralization between MNP and LDH. In detail, the negatively charged MNP replaced the relatively weaker electronegative groups of Cl^- and CO_3^{2-} between LDH layers by means of ion exchange, leading to the zeta potential decrease of MNP/LDH.

Photothermal characterization of LDH/MNP in vitro

The photothermal performance analysis of LDH/MNP in vitro were showed in Fig. 6. Figure 6(a) exhibited the temperature-time curve of LDH dispersions with concentration of 100 $\mu\text{g/mL}$ irradiated by laser for 5 min (wavelength 808 nm and laser power density of $1 \text{ W}\cdot\text{cm}^{-2}$), illustrating that the temperature of LDH stayed still as room temperature and did not significantly increased with the increasing of irradiated time. Hence, it is confirmed that LDH held no photothermal property. The temperature-time curves of LDH/MNP dispersions with different concentrations (0/25/50/100/150/300 $\mu\text{g/mL}$) under 5 min of laser irradiation (wavelength 808 nm and laser power density of $1 \text{ W}\cdot\text{cm}^{-2}$) was shown in Fig. 6(b). The results proved that at the same time point, the temperature became higher as the concentration of the LDH/MNP increased and the photothermal property of LDH/MNP was positively correlated with the concentration of LDH/MNP. Besides, when the concentration of LDH/MNP reached 300 $\mu\text{g/mL}$, the temperature of the dispersions reached 58.5°C after 5 min of irradiation, which was enough to achieve killing effect on cancer cells [49]. Combining the results in Fig. 1(a), it could be ensured that the photothermal property of LDH/MNP was generated by the interlamellar photothermal agent MNP.

After irradiation for 5 min under different laser power density of 0.5/0.75/1.0/1.25 $\text{W}\cdot\text{cm}^{-2}$ (wavelength 808 nm), the temperature-time curves of LDH/MNP (100 $\mu\text{g/mL}$) were summarized in Fig. 6(c). The temperature of MNP/LDH raised as the laser power density became higher. The experimental results proved that the photothermal characteristics of LDH/MNP were positively correlated with the laser power density. When the temperature raised enough to kill the cancer cell (usually $42\text{--}45^\circ\text{C}$ [49]), the laser power density could be chosen as the optimal one. In Fig. 6(c), when the laser power density was $0.75 \text{ W}\cdot\text{cm}^{-2}$, the temperature reached 44°C after 5 min of irritation and the optimal laser power density was $0.75 \text{ W}\cdot\text{cm}^{-2}$.

Figure 6(d) displayed the photothermal stability of LDH/MNP. Generally, the LDH/MNP dispersions of 100 $\mu\text{g/mL}$ were irradiated for 5 min and cooled naturally for 5 min under the conditions of wavelength 808 nm and power density of $1 \text{ W}\cdot\text{cm}^{-2}$. After 6 cycles

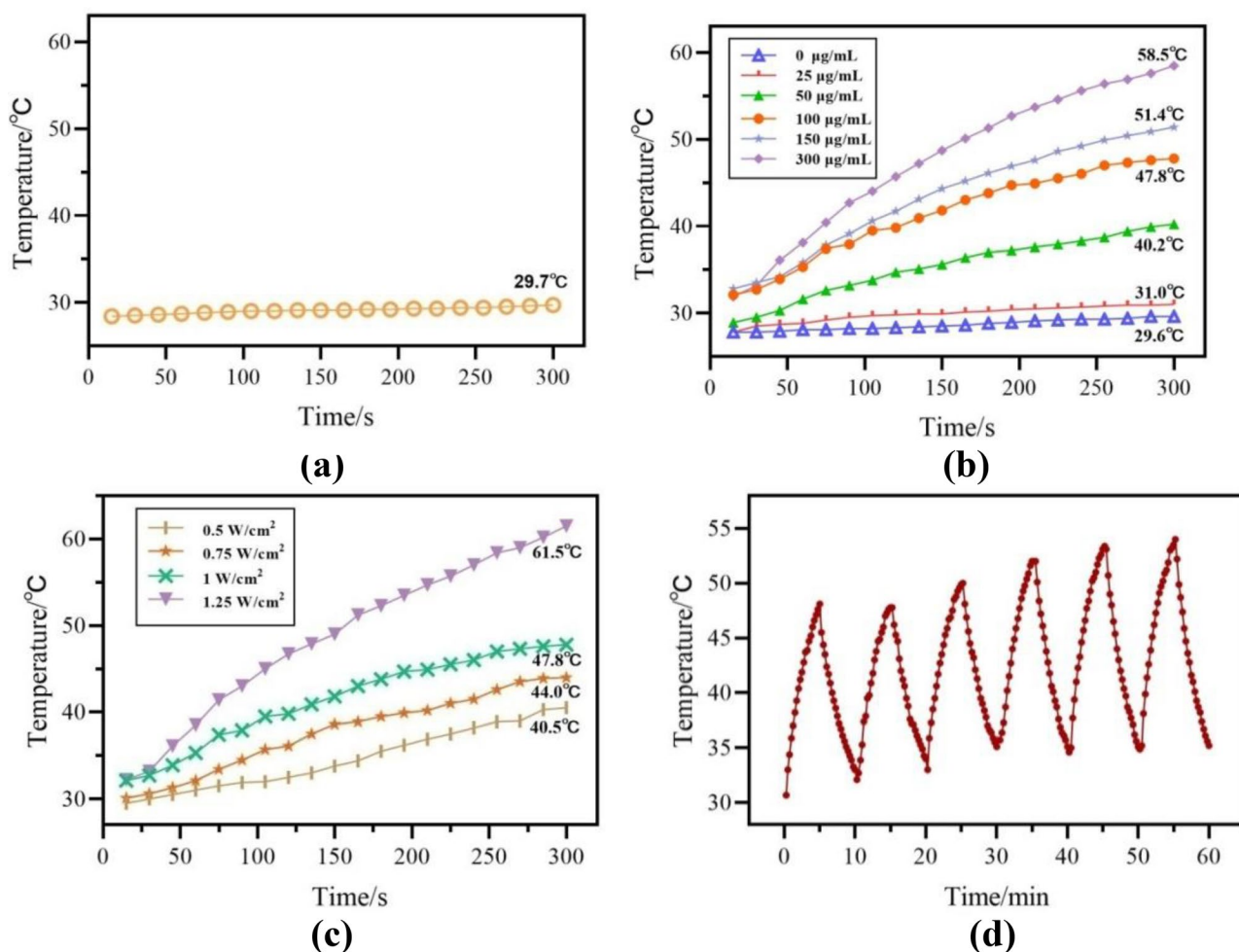


Fig. 6 (a) Temperature variation curve of LDH dispersions (100 $\mu\text{g/mL}$) (wavelength 808 nm, power density 1 $\text{W}\cdot\text{cm}^{-2}$); (b) Temperature variation curves of LDH/MNP dispersions under different concentrations (300/150/100/50/25/0 $\mu\text{g/mL}$) (wavelength 808 nm, power density 1 $\text{W}\cdot\text{cm}^{-2}$); (c) Temperature variation curves of LDH/MNP dispersions (100 $\mu\text{g/mL}$) at 808 nm wavelength and different power densities (0.5/0.75/1.0/1.25 $\text{W}\cdot\text{cm}^{-2}$); (d) Photothermal stability of LDH/MNP dispersions (100 $\mu\text{g/mL}$) after 6 cycles of laser irradiation (wavelength 808 nm, power density 1 $\text{W}\cdot\text{cm}^{-2}$)

of uninterrupted operation, it could be summarized that the temperature of LDH/MNP remained the same value in every single cycle, indicating the stable photothermal property of LDH/MNP. According to the series of photothermal property experiments above, LDH/MNP was proved with typical photothermal property and stability, and could be used as a novel photothermal agent in tumor photothermal treatments.

Cytotoxicity of LDH and LDH/MNP

The biocompatibilities of LDH and LDH/MNP were determined via CCK-8 and the results were shown in Fig. 7. With the concentration of LDH increasing from 10 $\mu\text{g/mL}$ to 1000 $\mu\text{g/mL}$, the average survival rate of LDH against normal H9C2 cells remained above 95%. This was due to the fine biocompatibility of LDH. Besides, as the concentration of LDH/MNP increased from 10 $\mu\text{g/mL}$ to 1000 $\mu\text{g/mL}$, the average survival rate

of LDH/MNP against normal H9C2 cells increased up to more than 100%. This phenomenon could be explained as that MNP was an amino acid derivative and could provide nutrients during cell growth in order to promote cell proliferation. Hence, it could be concluded that both LDH and LDH/MNP possessed fine biocompatibility and free of toxicity.

Conclusion

In this study, LDH was prepared via hydrothermal method, and the photothermal agent MNP was successfully intercalated between LDH layers via ion exchange method to acquire a novel stable photothermal system LDH/MNP. In the system of LDH/MNP, LDH acted as a functional carrier to load the photothermal agent MNP and enhance the stability, while MNP performed as the photothermal factor to endow the system with typical photothermal properties. Morphology characterization

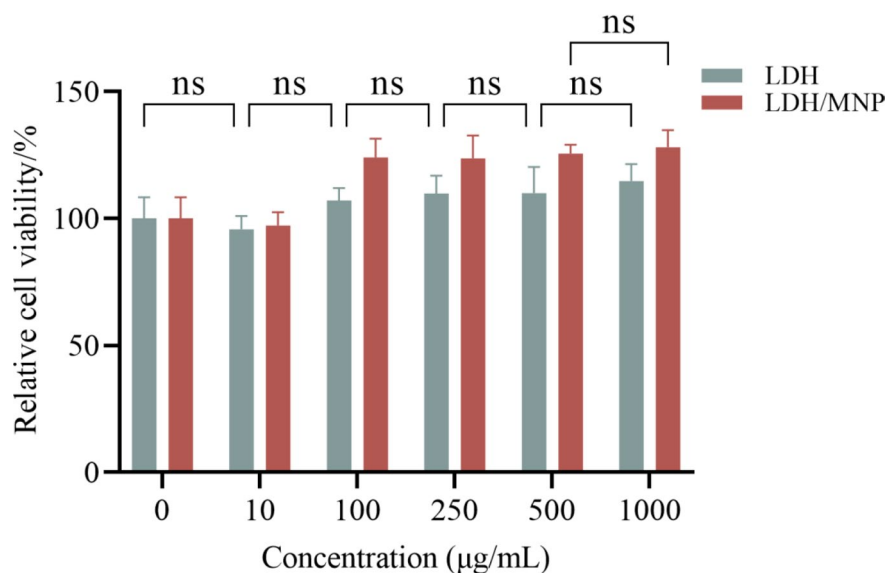


Fig. 7 Cell viability under different concentrations of LDH, LDH/MNP, incubated with normal cell H9C2

of TEM, XRD and FT-IR results confirmed the successful intercalation of MNP between LDH layers. The nanoparticle size distribution and PDI values further verified the stability and better particle distribution of LDH/MNP than MNP. The photothermal performance results showed that LDH/MNP possessed stable and typical photothermal characteristics. Cytotoxicity test proved that LDH/MNP was of fine cytocompatibility and free of toxicity. Therefore, LDH/MNP could be employed as a photothermal agent possessing better stability, favorable dispersions, typical photothermal properties and fine cell compatibility. LDH/MNP could replace MNP in field of photothermal therapy with stable property. The present research had laid a foundation for further studies on the efficient photothermal therapy of LDH/MNP in vivo.

Statistical analysis

All experiments were repeated at least three times for statistical analysis and the data were presented as means \pm standard deviation. One-way ANOVA with Bonferroni's correction was used to compare differences between at least three groups. In all pictures, no significance represented as ns, $P^* < 0.05$ represented one star, $P^{**} < 0.01$ represented two stars, $P^{***} < 0.001$ represented three stars, $P^{****} < 0.0001$ represented four stars.

Acknowledgements

We gratefully acknowledge the financial support provided by the Basic Research Program of Shanxi Province (NO: 202103021223237). Furthermore, the authors extend appreciation to Zujian Feng, a PhD from institute of Biomedical Engineering, Chinese Academy of Medical Science & Peking Union Medical College, for his valuable and thoughtful suggestions on the measurements and relevant problems of LDH/MNP.

Author contributions

X.L.: research idea conceptualization; supervised the study; data analysis; manuscript editing and funding acquisition. Y.W. and X.G.: investigation and

validation. J.S. and Y.L.: responsible for formal analysis and supervision. A.D. and R.Z.: contributed to resources, writing-review & editing. All authors read and approved the final manuscript.

Funding

This work has been financially supported by the Basic Research Program of Shanxi Province (NO: 202103021223237), National Natural Science Foundation of China (No: 82120108016, 82071987), Four Batches of Scientific Research Projects of Shanxi Provincial Health Commission (NO: 2020TD11, NO: 2020SYS15, NO: 2020XM10, NO: 2020XM49), Key Laboratory of Nano-imaging and Drug-loaded Preparation of Shanxi Province (NO: 202104010910010), Applied Basic Research Program of Shanxi Province (20210302124174).

Data availability

No datasets were generated or analysed during the current study.

Declarations

Ethics approval and consent to participate

Not applicable.

Consent for publication

Not applicable.

Competing interests

The authors declare no competing interests.

Abbreviations

LDH referred to layered double hydroxide and MNP referred to melanin nanoparticle in this article.

Received: 27 February 2024 / Accepted: 30 September 2024

Published online: 12 October 2024

References

1. Fujiwara K, Hasegawa K, Nagao S. Landscape of systemic therapy for ovarian cancer in 2019: primary therapy. *J Sci Cancer*. 2019;125:4582–6. <https://doi.org/10.1002/cncr.32475>.
2. Das P, Ganguly S, Margel S, Gedanken A. Tailor made magnetic nanolights: fabrication to cancer theranostics applications. *Nanoscale Adv*. 2021;3(24):6762–96. <https://doi.org/10.1039/d1na00447f>.

3. Véronique Debieu AD, Caluwé X, Wang, et al. Immunotherapy in breast cancer: an overview of current strategies and perspectives. *NPJ Brea Cancer*. 2023;9:7. <https://doi.org/10.1038/s41523-023-00508-3>.
4. Savas P, Salgado R, Denkert C, et al. Clinical relevance of host immunity in breast cancer: from TILs to the clinic. *Nat Rev Clin Oncol*. 2016;13:228–41. <https://doi.org/10.1038/nrclinonc.2015.215>.
5. Zhang K, Qi C, Kaiyong Cai. Manganese-based tumor immunotherapy. *Adv Mater*. 2023;35:2205409. <https://doi.org/10.1002/adma.202205409>.
6. Liu Y, Bhattarai P, Dai Z, Chen X. Photothermal therapy and photoacoustic imaging via nanotheranostics in fighting cancer. *Chem Soc Rev*. 2019;48:2053–108. <https://doi.org/10.1039/c8cs00618k>.
7. Zhi D, Yang T, O'hagan J, et al. Photothermal therapy. *J Controlled Release*. 2020;325:52–71. <https://doi.org/10.1016/j.jconrel.2020.06.032>.
8. Cui X, Ruan Q, Zhuo X, et al. Photothermal nanomaterials: a powerful light-to-heat converter. *Chem Rev*. 2023;123(11):6891–952. <https://doi.org/10.1021/acs.chemrev.3c00159>.
9. Liu Z, Cheng L, Zhang L, et al. Sub-100 nm hollow Au–Ag alloy urchin-shaped nanostructure with ultrahigh density of nanotips for photothermal cancer therapy. *Biomaterials*. 2014;35:4099–107. <https://doi.org/10.1016/j.biomaterials.2014.01.053>.
10. Malik S, Nemoto Y, Guo H, et al. Fabrication and characterization of branched carbon nanostructures. *Beilstein J Nano*. 2016;7:1260–6. <https://doi.org/10.3762/bjnano.7.116>.
11. Cote LJ, Cruz-Silva R, Huang J. Flash reduction and patterning of graphite oxide and its polymer composite. *J Am Chem Soc*. 2009;131:11027–32. <https://doi.org/10.1021/ja902348k>.
12. Lin C, Zhu Y. Dynamic photothermal-mechanical response of a microcantilever modified by carbon nanotube film. *Appl Opt*. 2016;55:2324–30. <https://doi.org/10.1364/AO.55.002324>.
13. Wang HY, Chang JJ, Shi MW, et al. A dual-targeted organic photothermal agent for enhanced photothermal therapy. *Angew Chem Int Ed*. 2019;58:1057–61. <https://doi.org/10.1002/anie.201811273>.
14. Abbas M, Zou Q, Li S, Yan X. Self-assembled peptide- and protein-based nanomaterials for antitumor photodynamic and photothermal therapy. *Adv Mater*. 2017;29:1605021. <https://doi.org/10.1002/adma.201605021>.
15. Huang X, Zhang W, Guan G, Song G, Zou R, J Hu. Design and functionalization of the NIR-responsive photothermal semiconductor nanomaterials for cancer theranostics. *Acc Chem Res*. 2017;50:2529–38. <https://doi.org/10.1021/acs.accounts.7b00294>.
16. Liu S, Pan X, Liu H. Two-dimensional nanomaterials for photothermal therapy. *Angew Chem Int Ed*. 2020;59:5890–900. <https://doi.org/10.1002/anie.201911477>.
17. Qin Jiang Y, Liu R, Guo, et al. Erythrocyte-cancer hybrid membrane-camouflaged melanin nanoparticles for enhancing photothermal therapy efficacy in tumors. *Biomaterials*. 2019;192:292–308. <https://doi.org/10.1016/j.biomaterials.2018.11.021>.
18. Jiang Q, Luo ZM, Men YZ, et al. Red blood cell membrane-camouflaged melanin nanoparticles for enhanced photothermal therapy. *Biomaterials*. 2017;143:29–45. <https://doi.org/10.1016/j.biomaterials.2017.07.027>.
19. Yang X, Fan B, Gao W, et al. Enhanced endosomal escape by photothermal activation for improved small interfering RNA delivery and antitumor effect. *Int J Nanomed*. 2018;13:4333–44. <https://doi.org/10.2147/IJN.S161908>.
20. Kim MA, Yoon SD, Lee CM. A drug release system induced by near infrared laser using alginate microparticles containing melanin. *Int J Biol Macromol*. 2017;103:839–44. <https://doi.org/10.1016/j.ijbiomac.2017.05.139>.
21. Guo LL, Li WY, Gu ZY, et al. Recent advances and progress on melanin: from source to application. *Int J Mol Sci*. 2023;24:4360. <https://doi.org/10.3390/ijms24054360>.
22. Ganguly S, Bhawal P, Choudhury A, et al. Preparation and properties of halloysite nanotubes/poly (ethylene methyl acrylate)-based nanocomposites by variation of mixing methods. *Polym-Plast Technol Eng*. 2018;57(10):997–1014. <https://doi.org/10.1080/03602559.2017.1370106>.
23. Ganguly S, Margel S. A review on synthesis methods of phyllosilicate- and graphene-filled composite hydrogels. *J Compos Sci*. 2022;6(1):15. <https://doi.org/10.3390/jcs6010015>.
24. Sideris PJ, Nielsen UG, Gan Z, et al. Mg/Al ordering in layered double hydroxides revealed by multinuclear NMR spectroscopy. *Science*. 2008;321:113–7. <https://doi.org/10.1126/science.1157581>.
25. Mishra G, Dash B, Pandey S. Layered double hydroxides: a brief review from fundamentals to application as evolving biomaterials. *Appl Clay Sci*. 2018;153:172–86. <https://doi.org/10.1016/j.clay.2017.12.021>.
26. Taviot-Guého C, Prévot V, Forano C, et al. Tailoring hybrid layered double hydroxides for the development of innovative applications. *Adv Funct Mater*. 2018;28:1703868. <https://doi.org/10.1002/adfm.201703868>.
27. Li Y, Bi HY, Li H, et al. Synthesis, characterization, and sustained release property of Fe₃O₄@(enrofloxacin-layered double hydroxides) nanocomposite. *Mater Sci Eng C*. 2017;78:886–91. <https://doi.org/10.1016/j.msec.2017.04.104>.
28. Bashir A, Malik LA, Ahad S, et al. Removal of heavy metal ions from aqueous system by ion-exchange and biosorption methods. *Environ Chem Lett*. 2019;17:729–54. <https://doi.org/10.1007/s10311-018-00828-y>.
29. Cao Y, Li G, Li X. Graphene/layered double hydroxide nanocomposite: properties, synthesis, and applications. *Chem Eng J*. 2016;292:207–23. <https://doi.org/10.1016/j.cej.2016.01.114>.
30. Chen W, Xing J, Lu Z, et al. Citrate-modified Mg–Al layered double hydroxides for efficient removal of lead from water. *Environ Chem Lett*. 2018;16:561–7. <https://doi.org/10.1007/s10311-017-0692-5>.
31. Cui PQ, Zhou HG, Li C, et al. Characteristics of using layered double hydroxides to reduce the VOCs from bituminous materials. *Constr Build Mater*. 2016;123:69–77. <https://doi.org/10.1016/j.conbuildmat.2016.06.117>.
32. Daud M, Hai A, Banat F, et al. A review on the recent advances, challenges and future aspect of layered double hydroxides (LDH) – containing hybrids as promising adsorbents for dyes removal. *J Mol Liq*. 2019;288:110989. <https://doi.org/10.1016/j.molliq.2019.110989>.
33. Chen X, Chai H, Cao Y, et al. Hierarchical CoGa layered double hydroxides grown on nickel foam as high energy density hybrid supercapacitor. *Chem Eng J*. 2020;38:1122620. <https://doi.org/10.1016/j.cej.2019.122620>.
34. Chen Z, Deng H, Zhang M, et al. One-step facile synthesis of nickel–chromium layered double hydroxide nanoflakes for high-performance supercapacitors. *Nano Adv*. 2020;2:2099–105. <https://doi.org/10.1039/d0na00178c>.
35. Dong X, Wang L, Wang D, et al. Layer-by-layer engineered Co–Al hydroxide nanosheets/graphene multilayer films as flexible electrode for supercapacitor. *Langmuir*. 2012;28:293–8. <https://doi.org/10.1021/la2038685>.
36. Liang H, Lin J, Jia H, et al. Hierarchical NiCo–LDH@NiOOH core-shell heterostructure on carbon fiber cloth as battery-like electrode for supercapacitor. *J Power Sour*. 2018;378:248–54. <https://doi.org/10.1016/j.jpowsour.2017.12.046>.
37. Xu ZP, Stevenson GS, Lu CQ, et al. Stable suspension of layered double hydroxide nanoparticles in aqueous solution. *J Am Chem Soc*. 2006;128:36–7. <https://doi.org/10.1021/ja056652a>.
38. Xu M, Wei M. Layered double hydroxide-based catalysts: recent advances in preparation, structure, and applications. *Adv Fun Mater*. 2018;28:1802943. <https://doi.org/10.1002/adfm.201802943>.
39. Song ZH, Yin Q, Yang SH, et al. A high-nickel layered double hydroxides cathode boosting the rate capability for chloride ion batteries with ultralong cycling life. *Small*. 2023;19. <https://doi.org/10.1002/sml.202302896>.
40. Lu Y, Jiang B, Fang L, et al. High performance NiFe layered double hydroxide for methyl orange dye and Cr(VI) adsorption. *Chemosphere*. 2016;152:415–22. <https://doi.org/10.1016/j.chemosphere.2016.03.015>.
41. Elmoubaraki R, Mahjoubi FZ, Elhalil A, et al. Ni/Fe and Mg/Fe layered double hydroxides and their calcined derivatives: preparation, characterization and application on textile dyes removal. *J Mater Res Tech*. 2017;6:271–83. <https://doi.org/10.1016/j.jmrt.2016.09.007>.
42. Jia Y, Zhang YS, Fu JG, et al. A novel magnetic biochar/MgFe-layered double hydroxides composite removing Pb²⁺ from aqueous solution: Isotherms, kinetics and thermodynamics. *Coll Sur Phys Eng Asp*. 2019;567:278–87. <https://doi.org/10.1016/j.colsurfa.2019.01.064>.
43. Wang J, Kang DJ, Yu XL, et al. Synthesis and characterization of Mg–Fe–La trimetal composite as an adsorbent for fluoride removal. *Chem Eng J*. 2015;264:506–13. <https://doi.org/10.1016/j.cej.2014.11.130>.
44. Wen T, Wu XL, Tan XL, et al. One-pot synthesis of water-swellaible Mg–Al layered double hydroxides and graphene oxide nanocomposites for efficient removal of As(V) from aqueous solutions. *ACS Appl Mater Inter*. 2013;5:3304–11. <https://doi.org/10.1021/am4003556>.
45. Anna R, Venera K, Vasily B, et al. Melanins from the lichens *lobaria pulmonaria* and *lobariaretigera* as eco-friendly adsorbents of synthetic dyes. *Int J Mol Sci*. 2022;23:15605. <https://doi.org/10.3390/ijms232415605>.
46. Li J, Yan L, Yang Y, et al. Insight into the adsorption mechanisms of aqueous hexavalent chromium by EDTA intercalated layered double hydroxides: XRD, FTIR, XPS, and Zeta potential studies. *New J Chem*. 2019;43:15915. <https://doi.org/10.1039/c9nj03479j>.
47. Shan R, Yan L, Yang Y, et al. Highly efficient removal of three red dyes by adsorption onto Mg–Al-layered double hydroxide. *J Ind Eng Chem*. 2015;21:561–8. <https://doi.org/10.1016/j.jiec.2014.03.019>.

48. Zhu X, Feng W, Chang J, et al. Temperature-feedback upconversion nano-composite for accurate photothermal therapy at facile temperature. *Nat Comm.* 2016;7:10437. <https://doi.org/10.1038/ncomms10437>.

Publisher's note

Springer Nature remains neutral with regard to jurisdictional claims in published maps and institutional affiliations.